The Astrophysical Journal, 758:119 (13pp), 2012 October 20 doi:10.1088/0004-637X/758/2/119

AN INTERPRETATION OF THE POSSIBLE MECHANISMS OF TWO GROUND-LEVEL ENHANCEMENT EVENTS

Kazi A. Firoz[1], W. Q. Gan[1], Y.-J. Moon[2], and C. Li[3]
[1] Key Laboratory of Dark Matter & Space Astronomy, Purple Mountain Observatory, Chinese Academy of Sciences, Nanjing 210008, China; kaziabulfiroz@pmo.ac.cn, kazifiroz2002@gmail.com
[2] School of Space Research, Kyung Hee University, 446-701 yongin-si, Gyeonggi-do, Republic of Korea
[3] School of Astronomy and Space Science, Nanjing University, Nanjing 210093, China
Received 2012 July 1; accepted 2012 August 26; published 2012 October 8

ABSTRACT

We have carried out this work to clarify the possible mechanisms of two important high-energy particle events (GLE69 2005 January 20, 06:46 UT and GLE70 2006 December 13, 02:45 UT). For this purpose, the cosmic-ray intensities registered by neutron monitors at several sites have been analyzed and studied with concurrent solar flares of different energy bands. To determine whether the ground-level enhancement (GLE) might be caused by the energy released from a solar flare or a CME-driven shock, we identify the particle injection time in terms of the lowest value of the spectral indices deduced from proton fluxes. If the GLE is caused by the energy released from particle acceleration in a solar flare, the intensive phase of the flare representing extreme emission should lie within the injection time. While fulfilling this criterion, it is further necessary to understand the possible relativistic energy computed in terms of the possible travel time deduced by employing the observational time lag between the GLE and the concurrent solar flare. Accordingly, we have found that GLE69 is procured with sufficient possible relativistic energy ($\sim$1.619 GeV) by the energy released from particle accelerations in the intensive phases of a solar flare components that have been corroborated by the injection time. The intensive phases of the flare components have also been justified with the prominent phases of a solar radio type III burst. For event GLE70, the particle injection time lies within the CME-driven shock justified by a solar radio type II burst which seems to be capable of procuring sufficient possible relativistic energies ($\sim$1.231 to $\sim$2.017 GeV). It is also noted that any fractional amount of energy ($\sim$0.226 to $\sim$0.694 GeV) from preceding flare components might be considered as a contribution to the shock acceleration process. Thus, GLE70 is presumably caused by the sum of the energy released mostly from a CME-driven shock and partially from preceding flare components.

Key words: acceleration of particles – cosmic rays – magnetic fields – Sun: coronal mass ejections (CMEs) – Sun: flares – Sun: magnetic topology – Sun: X-rays, gamma rays

Online-only material: color figures

1. INTRODUCTION

Ground-level enhancements (GLEs) are very high energetic particle events ($\geqslant$1 GeV) that appear conspicuously in the cosmic-ray intensity time-series profile as sudden, sharp and short-lived increases registered by neutron monitors (NMs) at different sites on the surface of the Earth. The intensity of the same GLE varies with respect to the geographical coordinates of the sites of the NMs and arrival direction of the particle. Characteristically, GLEs are the relativistic extension of solar energetic particle (SEP) events that behave distinctly differently from the general trend of cosmic rays, and can take place across any part of the profile irrespective of the solar maximum and minimum phases. Details can be studied in several papers (Cliver et al. 1982; Vashenyuk et al. 1993, 2003; Reames 1999; Bieber et al. 2004, 2008; Simnett & Roelof 2005; Martirosyan & Chilingarian 2005; Perez-Peraza et al. 2006; Bombardieri et al. 2008; Firoz et al. 2010).

Causal features of GLE events have been illustrated theoretically as well as observationally by many space researchers in the past (e.g., Kahler 1994; Klein et al. 1999; Gopalswamy et al. 2005; Cliver 2006; Wang & Wang 2006; Kuznetsov et al. 2006; Simnett 2006, 2007; Kocharov et al. 2007; McCracken et al. 2008; Moraal et al. 2008; McCracken & Beer 2008; Grechnev et al. 2008; Chupp & Ryan 2009; Masson et al. 2009; Matthiä et al. 2009; Reames 2009a, 2009b; Wang 2009; Vashenyuk et al. 2011). Most of these researchers commonly indicated that solar flare and coronal mass ejections (CMEs) are the principal drivers of a GLE. On this subject, Firoz et al. (2010) postulated characteristics of GLE-associated solar flares and CMEs, which revealed that GLEs are usually associated with wider high-speed CMEs and strong solar flares but the association does not clearly imply that these characteristics are responsible for GLEs. Thus, this study was extended with other parameters (solar, geophysical/interplanetary) which revealed that the time integration between a GLE and a simultaneous solar flare should be taken into consideration to understand the mechanism causing a GLE (Firoz et al. 2011a). This led to a study (Firoz et al. 2011b) on the time lag and cross-correlation between a GLE and a simultaneous solar flare. Although cross-correlation computations exposed strong correlations between the two, Firoz et al. still could not conclude that the strong correlations imply a causal relationship. In this circumstance, we focused explicitly on studying possible sources of energy for the GLE particles thereby proposing a paradigm (Firoz et al. 2011c) that was consistent with the suggestions of Aschwanden (2011).

The proposed paradigm determined possible relativistic energy in terms of the travel time of the particle deduced by employing the observational time lag between the peaks of the GLE and the concurrent flare. The criterion was that the observational time lag should be $\gtrsim$5 minutes because the time difference between the measurements of solar flare intensity

at the geostationary orbit and the GLE ($\geqslant$1 GeV) particle intensity on Earth's surface is supposed to be $\gtrsim$5 minutes. This criterion was consistent with the deduction of the velocity of the particle, which must be less than the velocity of light. Results suggested that GLE69 showed possible relativistic energy $\geqslant$1 GeV while GLE70 $\ll$ 1 GeV. Therefore, our present effort is to set up criteria that can justify whether a GLE is caused by the energy released from particle acceleration in a solar flare or a CME-driven shock. Toward that aim, we study concurrent solar radio bursts, chromospheric evaporation, and magnetic topology to gain a better understanding of particle accelerations in solar flares. Then we verify cross-correlations and corresponding time lags between the GLEs and flares. Finally, we deduce possible relativistic energies of the GLEs that can be justified by the injection criteria.

This study is based on a previous study (Firoz et al. 2011c) considering the same two events (GLE69, 2005 January 20, 06:46 UT and GLE70, 2006 December 13, 02:45 UT). This time we utilize the data for GLEs from several NMs and also discuss reasons for the variability.

2. DATA ANALYSIS

The Neutron Monitor Database (NMDB)[4] center (Klein et al. 2010; Mavromichalaki et al. 2011) holds 5 minute resolution data of cosmic-ray intensity (CRI) collected from different NMs at different sites around the world. For our two selected events (GLE69, 2005 January 20, 06:46 UT and GLE70, 2006 December 13, 02:45 UT), we have taken the pressure-corrected count rates (CRI) for the GLEs from the NMDB. The CRI varies due to latitudinal differences at different sites (see Figure 1 and Table 1), so we have studied the mean intensity as a reference intensity profile with low-energy proton fluxes to visualize the general trend. The profile has been composed with the concurrent hard X-ray (HXR) and soft X-ray (SXR) fluxes (Figure 2). The 1 minute resolution data of HXR utilized in the previous study (Firoz et al. 2011c) have been averaged into 5 minute resolution data for this study. Five-minute resolution data from the SXR and proton fluxes have been collected from NOAA's *GOES*[5] (e.g., Aschwanden & Freeland 2012).

The wavelengths of the flare components in different energy bands (keV) have been estimated (Table 2) by means of the usual Planck equation ($\lambda = hc/E$, in which λ is wavelength, h is Planck's constant, and c is the velocity of light).

Over a few energy bands during GLE70, time lag between the flare peak and GLE onset is not >5 minutes and consequently the velocity of the particle is greater than the velocity of light, which is unphysical. As a result, the possible relativistic energy cannot be deduced (marked as "NA" in Table 2). As an alternative, we have checked the travel time deduced by means of the time lag between onset of the flare and onset of the GLE depending on the argument that the HXR onset time is concomitant with the onset of a radio emission burst.

To fix the particle injection time, we consider the lowest value of the proton spectral indices. For this, a power-law spectrum (e.g., Li et al. 2009) has been applied. The power-law spectrum $f(E) \propto E^{-\gamma}$ defines the spectral index as

$$\gamma = -\frac{\log f(E)}{\log E}, \quad (1)$$

where E is the particle energy level, $f(E)$ is the function of energy for the time history of each energy level, and γ is the spectral index. We have used the proton fluxes for energy levels (E) > 10 MeV, >30 MeV, >50 MeV, and >100 MeV, and the time history data ($f(E)$) for each of those energy levels. Similarly, the power-law spectrum (Equation (1)) has also been exploited for electron fluxes (EPAM;[6] e.g., Cane et al. 2010) to identify the most prominent phase of the solar radio type III burst to better understand the extreme emission phase of the flare (Figure 3). The energy channels of the electron fluxes ($cm^{-2}\,str^{-1}\,s^{-1}$) we have studied are 0.038–0.053 MeV, 0.053–0.103 MeV, 0.103–0.175 MeV, and 0.175–0.315 MeV detected by DE30. (The detector DE30 lies at 30° from the spacecraft spin axis).

Instruments on *RHESSI*[7] providing the HXR data and WAVES[8] on the *Wind*[8] spacecraft supplying the solar radio bursts have been illustrated in our previous study (Firoz et al. 2011c). To examine spatial evolutions, we have studied flare images from *TRACE*[9] (e.g., Moon et al. 2004). Because of the unavailability of the data from *TRACE* for GLE70, we have used the data recorded by SOT/WB on *Hinode*[10] (e.g., Moon et al. 2007) for this GLE.

3. OBSERVATION AND DISCUSSION

3.1. Variation in the Intensity of a High-energy Particle Event

NMs register the intensities of cosmic rays (high-energy particles) having different cutoff rigidities that depend on the particle trajectory in the magnetosphere—the cosmic-ray particles undergo trajectories through interactions with magnetospheric fields and conserve energies in each step of the trajectory before registering on Earth, and the intensities of the particles vary depending on how many steps they encounter (e.g., Kudela & Usoskin 2004; Firoz 2006). Thus, the more the particle undergoes trajectory within the magnetosphere, the greater the amount of energy conserved and the more the cutoff rigidity and subsequently, the less the intensity of the particle. We can see (Table 1 and Figure 1) that the Lomnický štít (LMKS), having the highest cutoff rigidity, registered the lowest CRI whereas the OULU, having a lower cutoff rigidity, registered higher CRI.

Because of the asymptotic shape of Earth's magnetosphere, any tiny variation in CRI may also occur depending on different pitch angles (e.g., Miroshnichenko 2001; Perez-Peraza et al. 2008), and a small shift in time of the GLE peak at different NMs may take place. Thus, we can see (Table 1 and Figure 1) that the peak time of GLE69 varies between 07:00 (UT) and 07:06 (UT), while the peak time of GLE70 varies between 03:00 (UT) and 03:12 (UT). For both events (GLE69 and GLE70), Yakutsk (YKTK) has a much later peak time than the other NMs—for GLE69, the peak time (07:00 UT) at OULU was 6 minutes earlier than the peak time (07:06 UT) at YKTK while for GLE70 the peak time (03:00 UT) at LMKS was 12 minutes earlier than the peak time (03:12 UT) at YKTK (see Figure 1 and Table 1). So, considering the transport effect (e.g., Schlickeiser & Miller 1998), the mean of the intensities of cosmic rays denotes a reference intensity profile with a peak time at 07:04 UT for GLE69 and 03:05 UT for GLE70. This reference profile can be represented as high-energy proton (HEP) flux (GeV) at the

[4] http://www.nmdb.eu/
[5] National Oceanic Atmospheric Administration (NOAA): http://goes.ngdc.noaa.gov/
[6] http://www.srl.caltech.edu/ACE/ASC/level2/lvl2DATA_EPAM.html
[7] http://hesperia.gsfc.nasa.gov/rhessi/
[8] http://lep694.gsfc.nasa.gov/waves
[9] http://trace.lmsal.com/trace_cat.html
[10] http://darts.isas.jaxa.jp/solar/hinode/query.php

Table 1
Comparison of GLE Time and Peak Intensity at Seven Different NM Stations

Neutron Monitors	Altitude	Latitude	Longitude	Cutoff Rigidity	GLE69				GLE70			
	(m)	(°)	(°)	(GV)	Start (UT)	Onset (UT)	Peak (UT)	Intensity (I_r%)	Start (UT)	Onset (UT)	Peak (UT)	Intensity (I_r%)
LMKS	2634	49.20N	20.22E	3.84	06:46	06:53	07:05	20.637	02:46	02:52	03:00	10.626
MOSC	200	55.47N	37.32E	2.43	06:44	06:51	07:04	95.172	02:48	02:51	03:01	23.123
KIEL	54	54.34N	10.12E	2.36	06:45	06:52	07:05	93.774	02:47	02:51	03:01	34.133
YKTK	105	62.01N	129.43E	1.65	06:49	06:52	07:06	143.424	02:45	02:53	03:12	16.969
KERG	33	49.35S	70.25E	1.14	06:48	06:53	07:05	177.781	02:44	02:55	03:10	45.105
OULU	15	65.05N	25.47E	0.81	06:49	06:52	07:00	269.567	02:49	02:54	03:05	92.433
APTY	181	67.57N	33.4E	0.65	06:46	06:52	07:04	184.829	02:46	02:51	03:06	84.411
For the reference (mean) intensity					06:46	06:54	07:04	133.794	02:45	02:50	03:05	40.060

Notes. Altitude (m), latitude (°), longitude (°) and cutoff rigidity (GV) of the neutron monitors Lomnický Štít (LMKS), Moscow (MOSC), Kiel (KIEL), Yakutsk (YKTK), Kerguelen (KERG), Oulu (OULU), and Apatity (APTY) are noted. The start, onset, and peak times of the two important ground-level enhancement events (GLE69 and GLE70) are also noted to comprehend the latitudinal impact. (The criteria of fixed start and onset timings have been defined in Firoz et al. 2011c.) The mean value (I_r%) can be determined by considering the transport effect. (The peak intensity of GLE69 is about three times that of GLE70. This issue is consistent with the total radiation exposed by the proton fluence (Firoz et al. 2010) as well as the strength of the flares (Firoz et al. 2011b) and concomitant solar microwave/radio emission bursts (discussed in this paper).)

Table 2
Possible Travel Time, Velocity, and Relativistic Energy of the GLE Particle

Events	Concurrent Solar Flare Components			When Travel Time Is Deduced in Terms of Time Lag between Flare Peak and GLE Onset				When Travel Time Is Deduced in Terms of Time Lag between Flare Onset and GLE Onset			
	Type (w m^{-2})	Energy Bands (keV)	Wavelengths (Å)	dT_{fpgo} (minutes)	T_p (∼minutes)	V_p (∼km s^{-1})	E_g (∼GeV)	dT_{fogo} (minutes)	T_p (∼minutes)	V_p (∼ km s^{-1})	E_g (∼GeV)
GLE69	HXR	6–12	∼2.7–1.3	08	16.33	2.45e5	0.686	14	22.33	1.79e5	0.231
		12–25	∼1.3–0.50	06	14.33	2.79e5	1.619	12	20.33	1.97e5	0.304
		25–50	∼0.50–0.25	09	17.33	2.31e5	0.530	11	19.33	2.07e5	0.357
		50–100	∼0.25–0.123	09	17.33	2.31e5	0.530	11	19.33	2.07e5	0.357
		100–300	∼0.123–0.041	09	17.33	2.31e5	0.530	10	18.33	2.18e5	0.429
		300–800	∼0.041–0.015	08	16.33	2.45e5	0.686	10	18.33	2.18e5	0.429
		800–7k	∼0.015–0.002	08	16.33	2.45e5	0.686	10	18.33	2.18e5	0.429
	SXR	∼1.55–12.42	∼1.000–8.000	06	14.33	2.79e5	1.619	09	17.33	2.31e5	0.530
		∼4.14–24.84	∼0.500–4.000	09	17.33	2.31e5	0.530	14	22.33	1.79e5	0.231
GLE70	HXR	6–12	∼2.7–1.3	12	20.33	2.21e5	0.452	16	24.33	1.85e5	0.253
		12–25	∼1.3–0.50	17	25.33	1.78e5	0.226	19	27.33	1.65e5	0.184
		25–50	∼0.50–0.25	17	25.33	1.78e5	0.226	19	27.33	1.65e5	0.184
		50–100	∼0.25–0.123	05	13.33	3.38e5	NA	22	30.33	1.48e5	0.141
		100–300	∼0.123–0.041	05	13.33	3.38e5	NA	22	30.33	1.48e5	0.141
		300–800	∼0.041–0.015	05	13.33	3.38e5	NA	23	31.33	1.44e5	0.131
		800–7k	∼0.015–0.002	05	13.33	3.38e5	NA	08	16.33	2.76e5	1.433
	SXR	∼1.55–12.42	∼1.000–8.000	10	18.33	2.45e5	0.694	30	38.33	1.17e5	0.0813
		∼4.14–24.84	∼0.500–3.000	15	23.33	1.93e5	0.287	25	33.33	1.35e5	0.112

Notes. The table contains high-energy particle events (GLE69 and GLE70 over the mean intensity) and concurrent solar flare components of different energy bands (keV) with corresponding wavelengths (Å) for hard X-rays (HXRs) and soft X-rays (SXRs). The observational time lag (dT_{fpgo}) between flare peak and GLE onset has been exploited to determine the travel time (T_p) of the GLE particle and, consequently, the possible velocity along the spiral magnetic field line paths following the model of the previous work (Firoz et al. 2011c). The HXR and SXR flare components noted here have been displayed in Figure 2, which paves an opportunity to look into the temporal association between thermal and nonthermal emissions. For a few energy bands during GLE70, the time lag between flare peak and GLE onset is not >5 minutes and consequently the velocity of the GLE70 particle is more than the light velocity that is superfluous, and as a result the possible relativistic energy cannot be deduced (marked by "NA"). So, alternatively we have checked the travel time deduced by the observational time lag (dT_{fogo}) between flare onset and GLE onset.

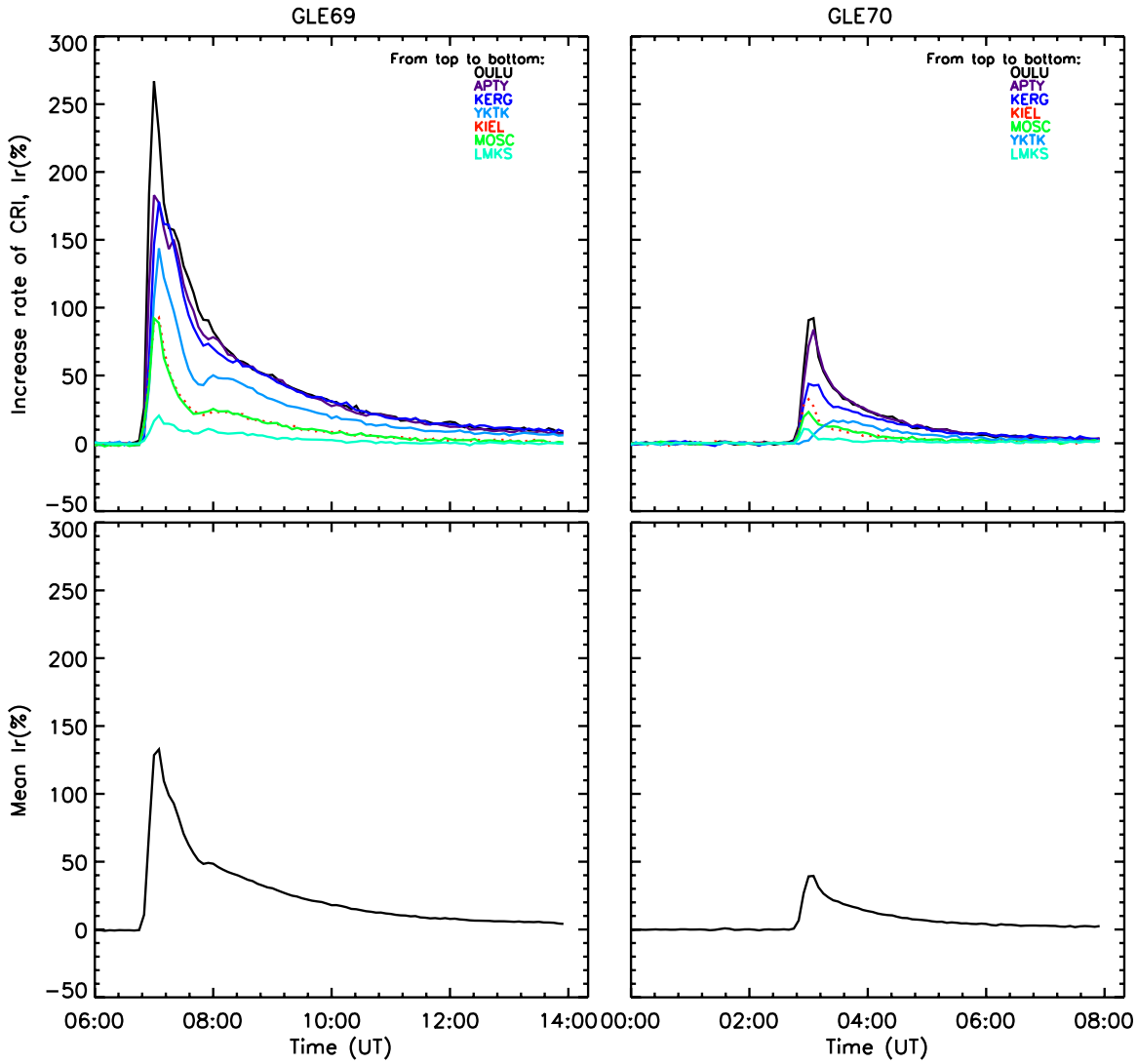

Figure 1. Increase rates (I_r%) of the intensities of 5 minute resolution high-energy proton (HEP) fluxes, known as cosmic rays, registered by NMs at different sites (Table 1), for the two events (GLE69 and GLE70) (top panel). The mean strength of the I_r (%) of 5 minute resolution cosmic-ray intensity (CRI) is also shown (bottom panel) to comprehend the general trend. The increase rate (%) is over the pre-event background and deduced by following the process given in Firoz et al. (2011b).
(A color version of this figure is available in the online journal.)

surface of the Earth with low-energy proton (LEP) flux (MeV) at the geostationary orbit to determine the temporal association between them (see Figure 2).

3.2. Particle Acceleration in Solar Flares and CME-driven Shocks during the Events

3.2.1. LEP and HEP Trends during Particle Acceleration

The trend of LEP (MeV) with HEP (GeV) during GLE69 differs from the trend during GLE70. The LEP fluxes have a strong impulsive phase nearly concurrent with the onset of GLE69 and then a gradual phase continues through the end of the event whereas for GLE70 the LEP fluxes have a weak impulsive rise that evolves very slowly (i.e., gradual–mixed–impulsive) followed by a continuous gradual phase. The gradual–mixed–impulsive phases of LEP fluxes for GLE70 can be called hybrid phases. This kind of event is supposed to consist of a mixture of flare-accelerated and CME-driven shock-accelerated particle populations (e.g., Kallenrode et al. 1992; Cliver 1996; Kocharov & Torsti 2002). However, for both events, during particle injection time, the LEP fluxes have growth phases (characterized by either an impulsive or hybrid phase) followed by gradual phases.

The most intensive phase of the LEP fluxes coincides with the lowest value of spectral indices (see Figure 2). It is found that the lowest value ($\gamma = 0.259$) of spectral indices during GLE70 is almost two times the lowest value ($\gamma = 0.141$) of spectral indices during GLE69. This gives a clear indication that the lower the spectral index, the stronger the particle injection and consequently, the stronger the GLE.

3.2.2. Injection Time during Particle Acceleration

The most intensive phases of the proton fluxes are inversely proportional to the lowest value of the spectral indices that can be considered as the particle injection time. In principle, the injection time should lie within the time when the energy releases from particle accelerations in a solar flare or CME-driven shock. Naturally, the particle injection time does not lie along the intensive phase of a flare and a shock wave at the same time (see Figure 2). We believe the GLE occurs with respect to

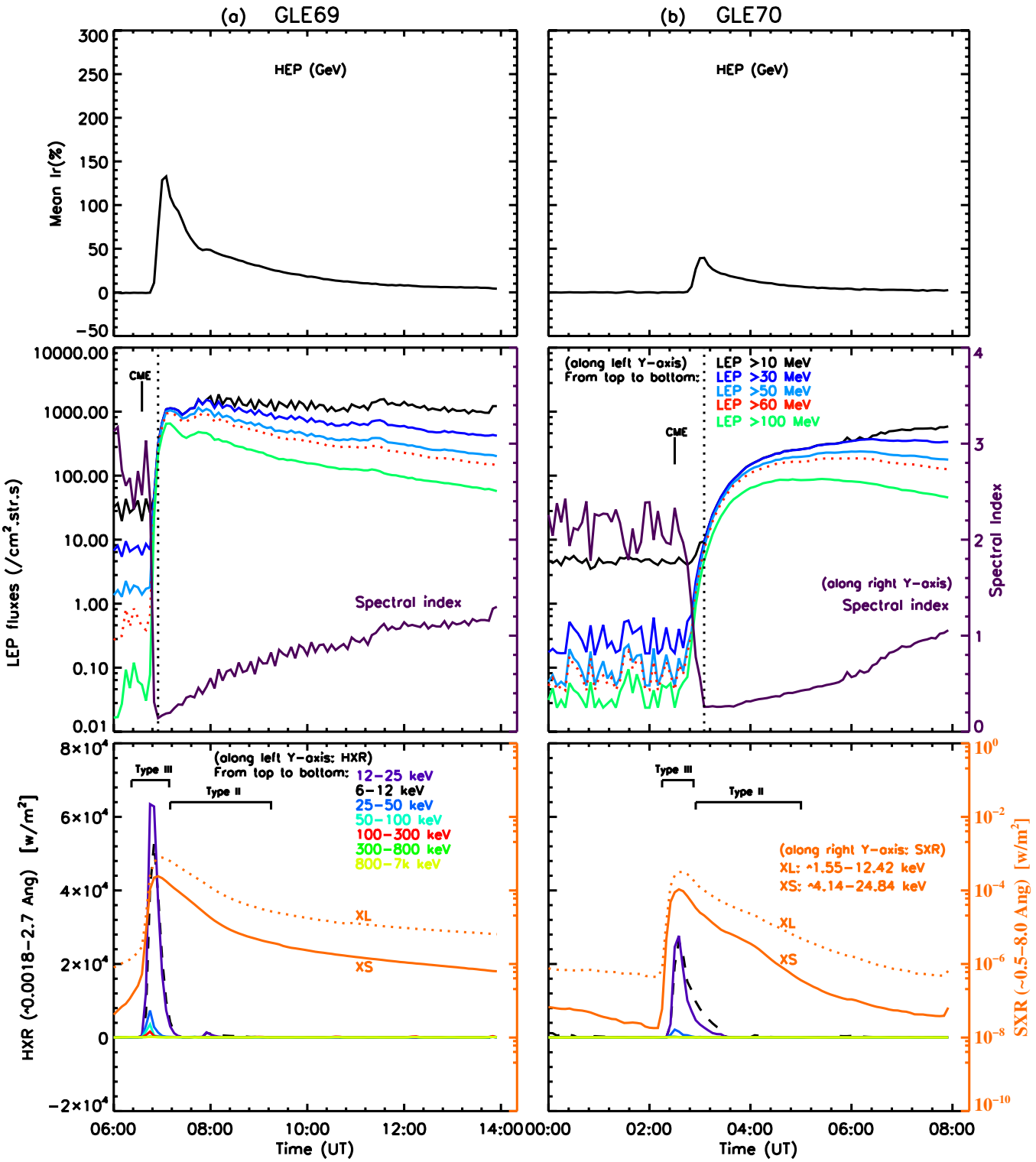

Figure 2. Mean strength (I_r%) of the intensities (top panel) of high-energy proton (HEP; cosmic-ray particles) are composed with the same (5 minute) resolution low-energy proton (LEP) fluxes (middle panel), and hard X-ray (HXR)/soft X-ray (SXR) fluxes (bottom panel). XL (∼1.55–12.42 keV) is the SXR of the longer wavelength and XS (∼4.14–24.84 keV) is the SXR of the shorter wavelength (see Table 2). The dotted lines parallel to the *y*-axis indicate the particle injection time identified in terms of the lowest value of the spectral indices. Durations of type III and type II bursts are considered in accordance with Figure 3.

(A color version of this figure is available in the online journal.)

the acceleration process (flare or CME-driven shock) within which the injection time lies.

If the intensive phases of flare components exist within the injection time, it is reasonable to argue that the energy released from the flares might cause the GLE. This is evident in Figure 2(a) for GLE69. It should further be checked whether any of those flare components accumulates possible relativistic energy $\geqslant$1 GeV. If the flare procures enough relativistic energy but particle injection time lies within the CME-driven shock wave, it is unclear whether the energy released from the flare

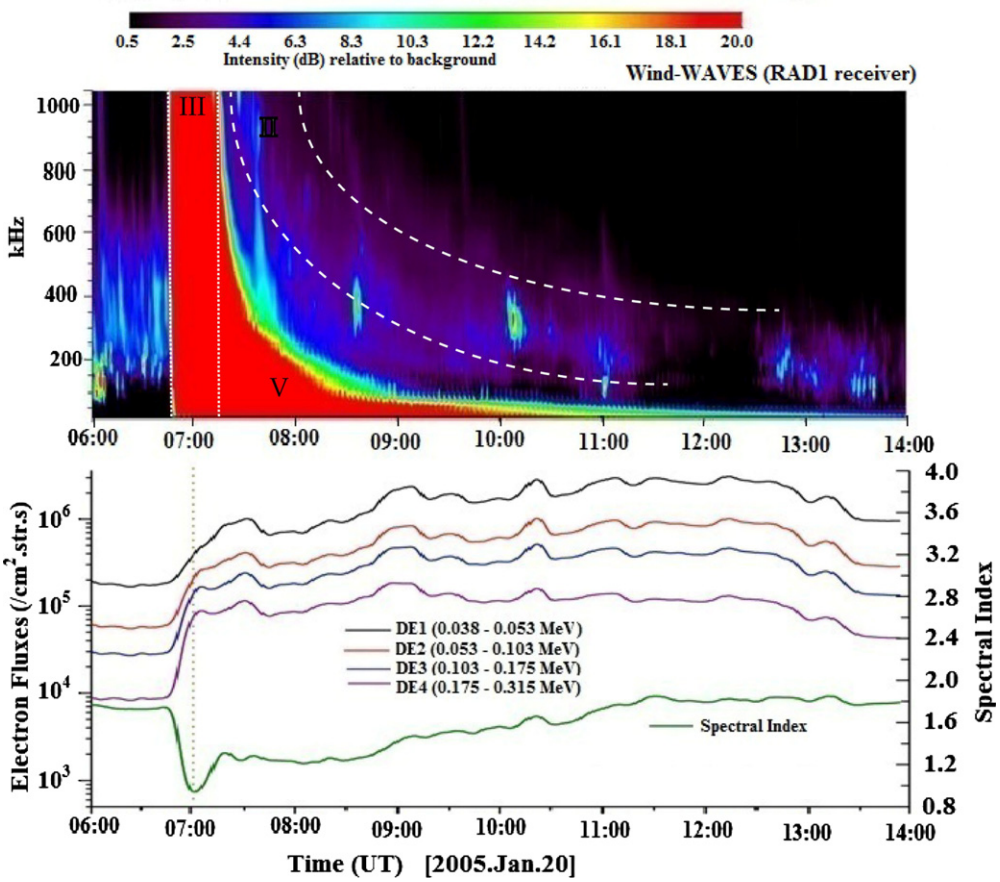

Figure 3. Solar radio bursts that took place during the GLEs (GLE69 and GLE70) associated with solar flares are displayed with simultaneous electron fluxes (the lowest value of the spectral indices of the electron fluxes denotes the most prominent phase of the type III radio burst). (a) A dynamic type III burst (06:45–07:20 UT) associated with extreme emissions of flares is seen as prominent during the intensive phase of GLE69. The type II burst (07:21–09:00 UT) appears to be dynamic after the decay phase of the flare. (b) The type III burst (02:30–2:45 UT) associated with flares is seen as prominent but much earlier than the intensive phase of GLE70. The type II (02:45–5:00 UT) burst concomitant shock wave is seen as dynamic along the intensive phase of the GLE70.

(A color version of this figure is available in the online journal.)

can cause the GLE. In this case, we consider that the energy released from the particle acceleration in the CME-driven shock wave causes the GLE. This is evident in Figure 2(b) for GLE70.

3.2.3. Phases of the Flare and CME-driven Shock during Particle Acceleration

As the shock approached, the magnitude of spectral indices became lower than the magnitude during the CME appearing time (Figure 2). Although, during both events, the first appearances of the CME were observed across a higher value of spectral indices, there was a good time difference between the first appearance of the CME and onset of the shock (Firoz et al. 2011b, 2011c). This can be realized with the first appearance of the CME (pointed in Figure 2) and shocks considered preferably in terms of a type II burst (Figure 3). As seen from the figure, a mild CME-driven shock started well after the peak in GLE69 (Figure 3(a)) and consequently, the energy released from the shock could not dominate the impulsive phase of GLE69. The coincidence of the solar flare with the phase of the lowest value of spectral indices revealed that the energy released from the particle acceleration in a solar flare has the greatest probability of causing GLE69 (Figure 2). With a similar point of view on GLE70, we see that the particle injection occurred much later (∼30 minutes) than the flare emission peaks. In this case, the particle injection coincides with the radio type II burst, so the energy released from the particle acceleration in a CME-driven shock has a possible chance of causing GLE70.

3.2.4. Scenario of Relativistic Electrons during Particle Acceleration

Electrons originating from flare sites are usually characterized in radio emission bursts and the most prominent phase of the type III burst coincides with the extreme emission phase of HXRs. So, HXR flares and concurrent radio emission observations are essential parameters for investigating the electron acceleration in flares (e.g., Kallenrode 1993; Mann, Classen & Aurass 1995; Wang et al. 2003; Klein et al. 2011).

We have exploited the lowest spectral index of the electron fluxes to identify the most prominent phase of type III burst (Figure 3). As found during GLE69, the spectral index (0.917) of electron fluxes is lower than the spectral index (1.221) of electron fluxes during GLE70, indicating that the injection of electron beams into the interplanetary space during GLE69 was much stronger than during GLE70. The result is consistent with the evidence that the type III burst during GLE69 is proportionally much wider/and more prominent than during GLE70. After the impulsive phase of electron fluxes, there seems to be more than one episode of fluctuations in electron fluxes that are concurrent with a radio type II burst. These episodes designate weak precipitations of (likely thermal) electrons traced by a weak radio emission burst (see Figure 3).

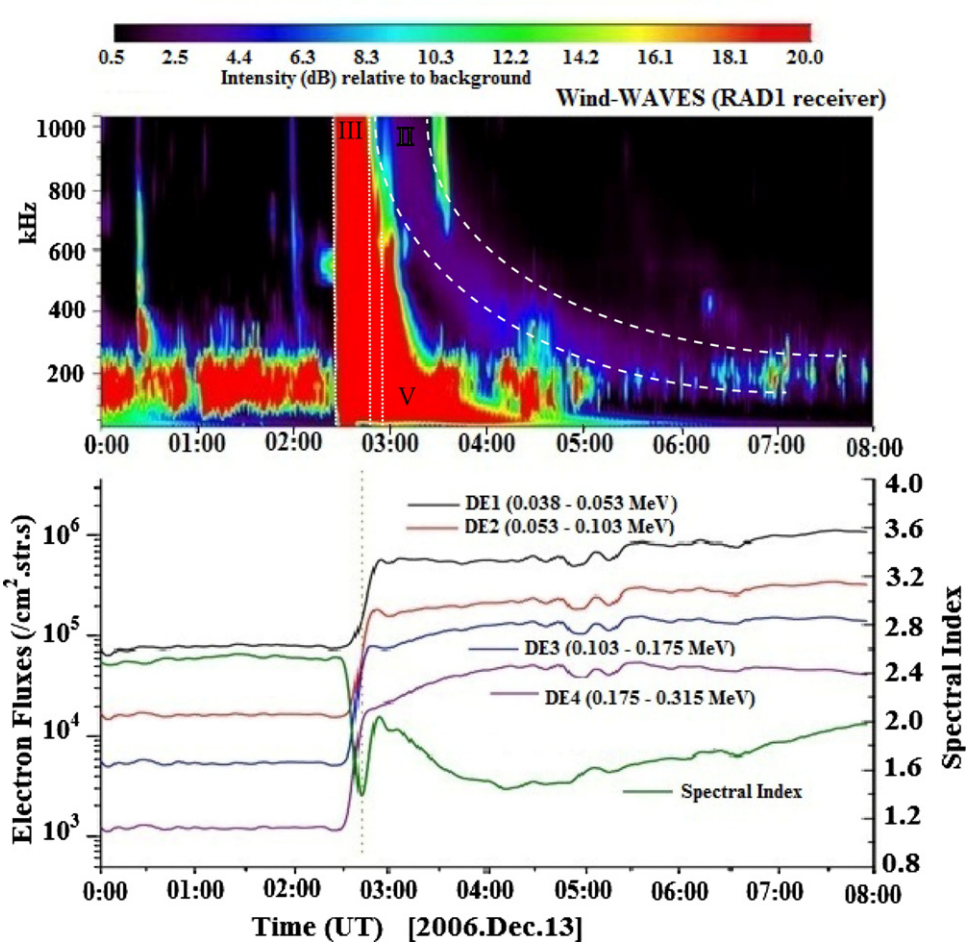

Figure 3. (Continued)

During GLE69 the intensive phase of the type III burst underwent longer fast drift from high to low frequencies, occurred singularly, and ended with a smooth continuum low-frequency type V burst (Figure 3(a)). The most prominent phase coincides with the intensive phases of HXR flares, implying that the energy released from a high-energy flare might have caused GLE69. For GLE70, although similar characteristics of electron fluxes are observed, the most prominent phase of the type III burst is much (∼25 minutes) earlier than the intensive phase of the GLE (see Figures 2(b) and 3(b)). In fact, there is mild type II burst across the onset that became prominent over the intensive phase of GLE70, indicating that the energy released from a CME-driven shock possibly caused GLE70.

During GLE70 the intensive phase of the type III burst underwent multiple shorter fast frequency drift. There might have been a sort of harmonic plasma emission—well before the GLE70 peak time, the first harmonic phase (∼1050 kHz) almost ended at the lowest frequency and the second harmonic phase (∼800 kHz) ended at the lowest frequency. Although there seems to have been a third harmonic phase, it ended within the initial phase of a type V burst (Figure 3(b)) that extended over the CME-driven shock.

3.2.5. Chromospheric Evaporation during Particle Acceleration

HXRs are widely believed to be nonthermal emission produced by high-energy electrons precipitating into the chromosphere. The thermalization of precipitating nonthermal emission leads to the formation of hot dense plasma that evaporates into the corona to form loops that emit at SXR wavelengths. More clearly, accelerated electrons generate HXRs and the continued flows of the (decelerated) electrons heat the plasma that subsequently generates the SXRs. (This is why peaks of HXR fluxes are usually earlier than those of the SXR fluxes; see Figure 2.) The heated plasma then expands outward along the flare loops thereby resulting in chromospheric evaporation (e.g., Gan et al. 1991; Warren & Antiochos 2004; Kumar et al. 2010).

Accordingly, the chromospheric evaporation might be the consequence of the interaction between thermal and nonthermal emissions (e.g., Figure 6). This means that the time difference between extreme emission phases of SXR and HXR fluxes can be considered as the duration of chromospheric evaporation, and that the later the SXR is compared to the HXR, the longer the chromospheric evaporation or, in other words, the longer the flaring loop, the longer the chromospheric evaporation (e.g., Aschwanden et al. 1995, 1998; Li & Gan 2006). Thus, we can surmise from the results presented in Figure 4 that the GLE69-associated flare has longer chromospheric evaporation than that of the GLE70-associated flare, indicating that the GLE69-associated flare has faster magnetic reconnection in the corona than the GLE70-associated flare.

3.2.6. Magnetic Configuration during the Particle Acceleration Processes

The GLE69-associated flare (X7.1) has a relatively simple magnetic configuration ($\beta\delta/\beta\gamma$), originating from the northwest active region (N14W61), and situated near the Sun–Earth

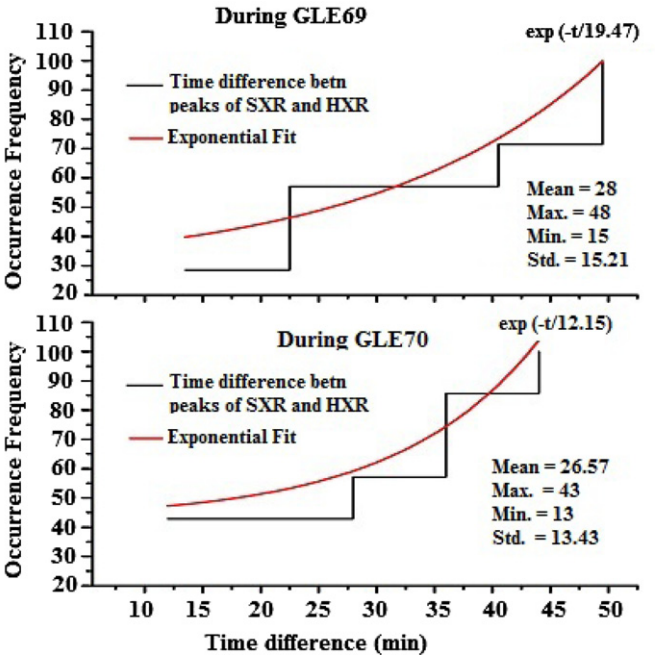

Figure 4. Histograms of observational time lags between peaks of hard X-ray (HXR) and longer wavelength (XL) soft X-ray (SXR) flares that occurred during the two specific events (GLE69 and GLE70). The temporal time difference between SXR and HXR flares is considered as the duration of chromospheric evaporation (see Figure 6). More details on chromospheric evaporation can be found in Li & Gan (2006).

(A color version of this figure is available in the online journal.)

connecting magnetic field lines (Firoz et al. 2011b). This flare is produced with two ribbons (Figure 5(a)) undergoing a fast magnetic reconnection at a lower coronal altitude (Figure 6(a)). By comparison, the GLE70-associated flare (X3.4) has a complex magnetic configuration ($\beta\gamma\delta/\beta\gamma\delta$), originating from the southwest active region (S06W23) of the Sun and situated about 40° away from the Sun–Earth connecting magnetic field lines (Firoz et al. 2011b). This flare also has two ribbons (Figure 5(b)) undergoing slower magnetic reconnection at a higher coronal altitude (Figure 6(b)). These findings are in line with those of a few researchers (Kocharov & Kovaltsov 1986; Cane 2002; Kocharov & Torsti 2002) who suggested that the prompt event and delayed event might originate from low and high coronal altitudes, respectively.

As observed (Figure 6), the reconnected field lines form flare loops with a cusp-shaped structure. The upward outflow generated from the reconnection site excites the flux ropes, causing filament eruption that subsequently ejects mass from the corona. The speed of the mass ejection depends on how much the filament is excited and on the loss of equilibrium due to the upward flow whose strength crucially depends on the position of the reconnection site across the corona. Accordingly, we can see (Figure 6(a)) that the downward outflow heavily precipitated the loops and flare emissions might escape through open field lines; the upward outflow from lower altitude becomes weak at higher altitude and the filament is weakly excited, so it causes slow ejection of coronal mass (882 km s^{-1}). In contrast, we can see (Figure 6(b)) that the downward outflow has weak precipitations (presumably one portion of the precipitated emissions escaped along the open field lines and the other portion was trapped beneath the CME) while the upward outflow from higher altitude heavily excites the filament, causing fast ejection of coronal mass (1774 km s^{-1}).

3.3. Cross-correlation between GLEs and Concurrent Solar Flares

Observationally (comparing Figure 2 with Figure 1 for all selected sites), the peak of GLE69 is more closely time-integrated (10–20 minutes) with extreme emissions of concurrent solar flares while the peak of GLE70 is not closely time-integrated (25–140 minutes) with extreme emissions of concurrent solar flares. This is an indication that the flare emission might be much more effective for GLE69 than for GLE70. This statement is also compatible with the evidence that the particle injection time coincides within the extreme emissions of flares

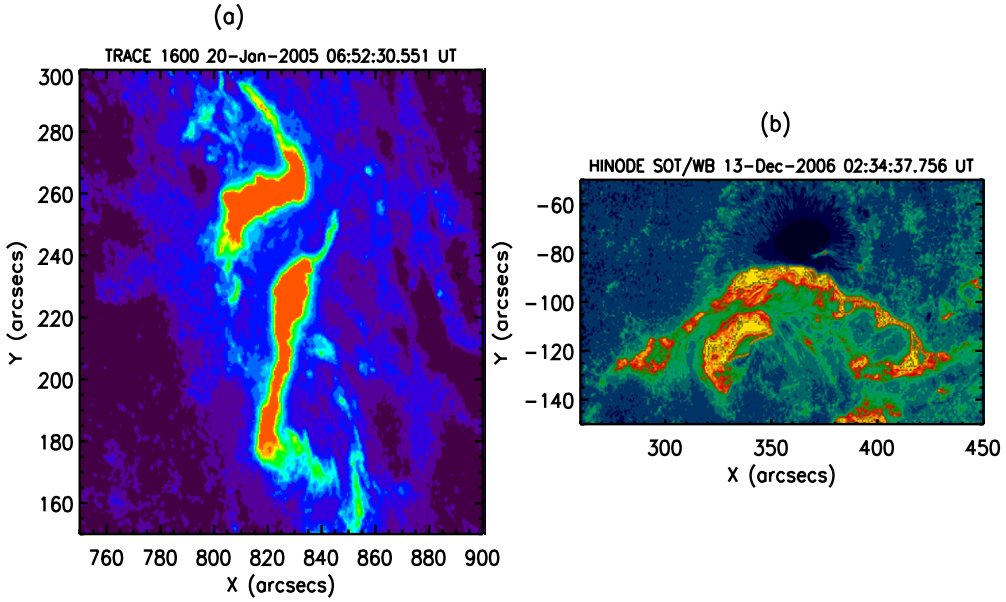

Figure 5. Ribbon structures of the GLE69- and GLE70-associated solar flares.(a) GLE69-associated flare (1600 Å X7.1/3B N14W61) image is processed from *TRACE*.[9] (b) GLE70-associated flare (195 Å X3.4/3B S06W23) image is processed from *Hinode*.[10]

(A color version of this figure is available in the online journal.)

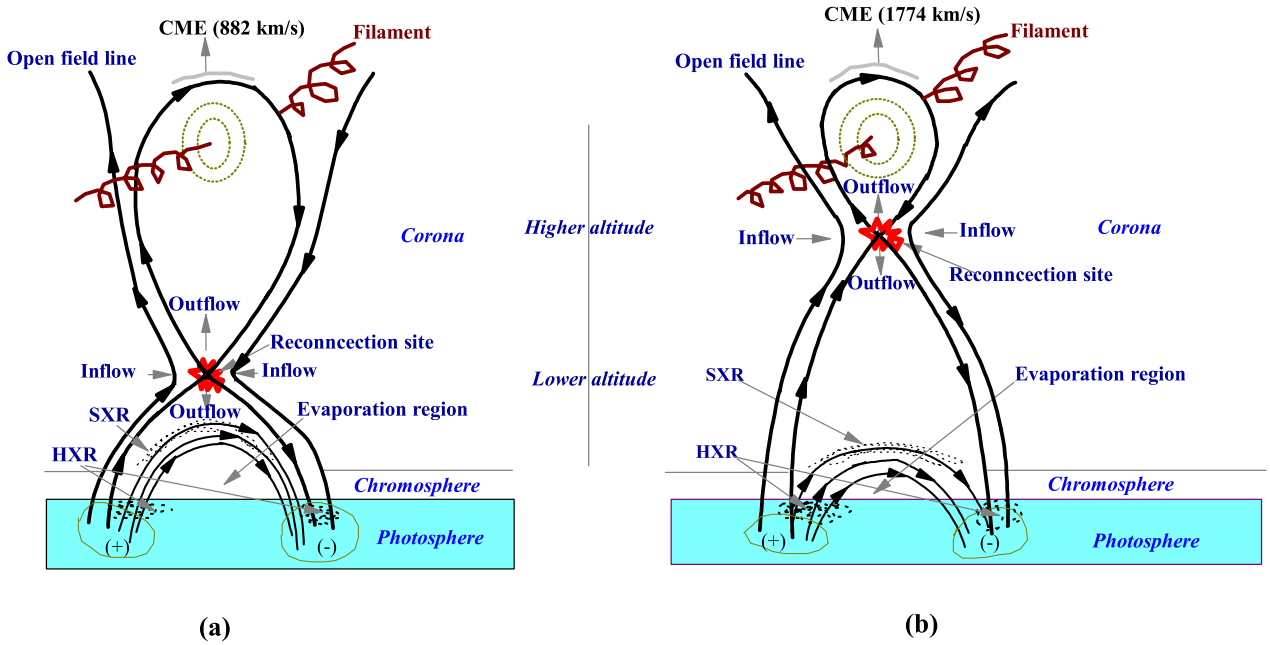

Figure 6. Schematic overview of the magnetic field lines of (a) the GLE69-associated flare and (b) the GLE70-associated flare. (a) Magnetic reconnection occurred at a lower coronal altitude and the filament triggered a less fast CME (882 km s^{-1}). (b) Magnetic reconnection occurred at a higher coronal altitude and the filament triggered a very fast CME (1774 km s^{-1}). (Speeds of CMEs are given in Firoz et al. 2010.) Details about the magnetic field line structures can be studied in several papers (Perez-Peraza et al. 1991; Moon et al. 1999; Asai et al. 2006; Li et al. 2007; Gan, Li & Miroshnichenko 2008; Aschwanden 2008).

(A color version of this figure is available in the online journal.)

during GLE69 whereas during GLE70 the injection time is much (∼30 minutes) later than the extreme emissions of the flares (see Figure 2).

So, the time corresponding to the highest correlation between GLE70 and a flare may reasonably be much longer than the time corresponding to the highest correlation between a flare and GLE69. (One component ⩾800 keV of the flares may be effective for GLE70 as it is more closely time-integrated.) Since the magnetic field reconnection time is supposed to be within the span of extreme emission from a flare and the prominent phase of a type III burst, we can theoretically look into the temporal cross-correlation and corresponding time lag to understand the role of flare emission in producing the GeV particles of the GLE event.

Following the cross-correlation method employed in the past studies (Firoz et al. 2011b, 2011c), we have checked the temporal correlations of GLE69 and GLE70 with concurrent HXR and SXR fluxes (Figure 2). In most of the cases, we have found strong correlations. The correlations found are in the range of 0.80–0.99 for both events except for a few cases—for LMKS, the correlation between GLE69 and 25 keV HXR is 0.684, and similarly for APTY, MOSC, and KIEL the correlations between GLE70 and 25 keV HXR are 0.795, 0.775, and 0.764, respectively. The reference intensity of GLE69 and GLE70 maintained the best correlations 0.89–0.99 (except for 300 keV HXR with GLE70), when the statistical time lags (dT_s) for GLE69 are between 40–95 minutes and for GLE70 between 40–145 minutes. For the reference intensity, the observational time lags (dT_o) between peaks of GLE69 and simultaneous flare components are 15–20 minutes while for GLE70 they are within the range of 30–40 minutes. These data are presented in Figure 7.

3.4. Possible Relativistic Energy of the GLE Particles

Following the model employed in our previous work (Firoz et al. 2011c), we have deduced the possible relativistic energies of GLE69 and GLE70. The travel time of the GLE particle is deduced in terms of the observational time lag between flare peak and GLE onset. Our previous work exploited the time lag between the GLE peak and flare peak, and similarly we also check possible relativistic energy for all selected sites.

For NM at Oulu, the possible relativistic energy showed up almost the same as before (see Firoz et al. 2011c), but for other NMs, the possible relativistic energy is ≪1 GeV. Investigation of the reference intensity also showed possible relativistic energy ≪1 GeV. This motivated us to look into the possible relativistic energy by using the time lag between the flare peak and GLE onset (see Table 2). As found, there are two possibilities for GLE69: energy from HXR (12–25 keV) and/or SXR (1.55–12.42 keV) might have been ∼1.619 GeV.

For GLE70, using the time lag between the flare peak and GLE onset, we have not found enough relativistic energy ⩾1 GeV (see Table 2). So, we have checked the possible relativistic energy in terms of the time lag between the flare onset and GLE onset (presuming that the flare onset may by chance

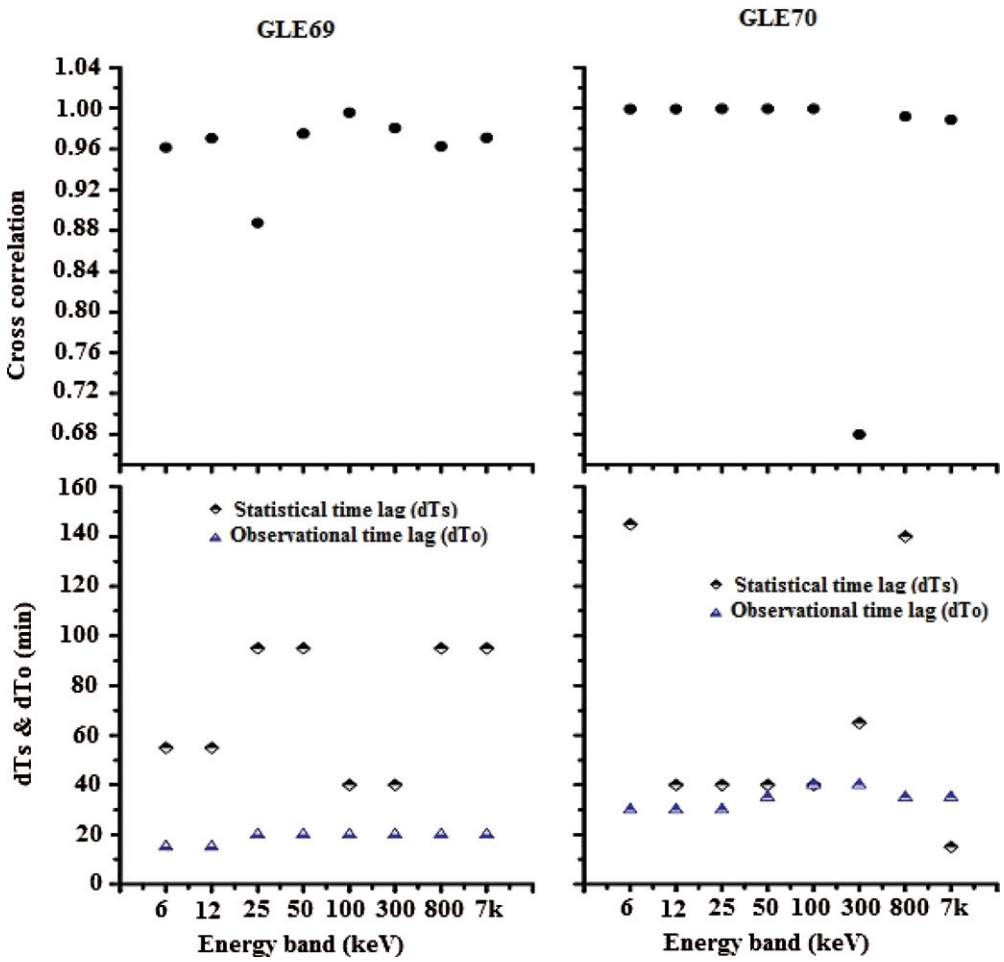

Figure 7. Cross-correlations of the reference intensity of GLE69 and GLE70 with concurrent HXR flares are exhibited in the top panels. (Along the *X*-axis are the energy bands of the flare components.) Statistical time lag (dT_s) and observational time lag (dT_o) are exhibited in the bottom panels. The dT_s is the time lag for cross-correlation and it is considered at the point where the highest correlation between GLEs and HXR fluxes is detected. dT_o is the observational time difference between peaks of GLEs and HXR fluxes. An illustration of the cross-correlation method has been given in Firoz et al. (2011b, 2011c).

(A color version of this figure is available in the online journal.)

cause GLE onset). In this case, only the γ-ray flares $\geqslant$800 keV procured possible relativistic energy $\sim$1.433 GeV. (According to *RHESSI*,[7] the HXR $\geqslant$500 keV can be considered[11] as γ-ray).

The CME-driven shock from the type II burst that started at 02:30 UT seems to have been spontaneous from 02:45 and became prominent within 02:50–03:00 UT (Figure 3(b)), and the time delay between the GLE70 peak and the CME-driven shock is observationally within 5–15 minutes. Thus, we see that the shock wave might enable particle acceleration over a wide range of heliolongitude (e.g., Cane 2002). So, if we consider the energy released from the particle acceleration across the shock, we can accept the possible relativistic energy $\geqslant$1 GeV in terms of any of these observational time lags (5–15 minutes). For instance, with the time lags (11 minutes and 12 minutes) between the CME-driven shock and the GLE70 peak, the possible relativistic energies are $\sim$1.231 and $\sim$2.017 GeV. That means the possibility of GLE70 being caused by the energy released from particle acceleration in the CME-driven shock can be accepted while any fractional amount of energy $\sim$0.226 to $\sim$0.694 GeV (Table 2) from preceding flare components might be considered as a contribution to the shock acceleration process.

[11] Private Communication with Dr. Kim Tolbert of *RHESSI* in 2011.

4. GENERAL DISCUSSION

Earlier, Firoz et al. (2011a) concluded that CME-driven shocks may modulate cosmic rays either directly or inversely, indicating that the energy released from a CME-driven shock may sometimes cause a sudden enhancement in cosmic-ray intensity (i.e., GLE). Another view of Cliver et al. (1982) noted by Perez-Peraza et al. (2009) is that the onset of a type II burst is the marker of relativistic proton acceleration, i.e., a shock wave may yield relativistic SEP. In this context, it can be noted that a CME that is not associated with a type II radio burst might not produce relativistic SEPs (Kocharov & Torsti 2002). This indicates that a CME-driven shock might be able to produce relativistic SEPs. All these statements are consistent with our findings. However, the suggestions of a few researchers (e.g., Vashenyuk et al. 2009; Miroshnichenko et al. 2009) pointed out by Kahler (2012) indicated that a CME-driven shock contributes only non-relativistic SEPs, so that both prompt and delayed/extended phases are attributed to flare processes. This statement contradicts GLE70 in view of the injection criteria.

Although we have found a possibility for relativistic energy $>$1 GeV in the case of a high-energy flare $\geqslant$800 keV, this does not satisfy the criteria of particle injection time. Hence, we argue that the energy released from particle acceleration in a CME-driven shock is mostly responsible for GLE70 while a fractional

amount of the energy released from preceding flare components can be considered as a contribution to the shock acceleration. This means that no unique acceleration process (either shock or flare alone) seems to be responsible for GLE70 (e.g., Masson et al. 2009).

5. SUMMARY AND CONCLUSION

In this study, we have interpreted the possible mechanisms of two GLE events (GLE69 and GLE70). We showed general trends of the two GLE events with simultaneous proton fluxes and flare components of different energy bands. Then we identified the particle injection time in terms of the lowest value of spectral indices deduced from proton fluxes. To understand the particle acceleration in solar flares and/or in CME-driven shocks, we studied exclusively the concurrent solar radio bursts and corresponding electron fluxes. For a better understanding of the concurrent solar flares, we presented chromospheric evaporation, flare ribbon structure, and magnetic field reconnection.

For the interpretation of the two GLE events we used the following criteria.

1. If the particles are injected from the solar flare site, the particle injection time should coincide with the impulsive phase of flares as observed in soft and hard X-rays.
2. If type III solar radio bursts occur during the impulsive phase of a solar flare, relativistic particles with energies $\geqslant$1 GeV may also be produced that could in turn produce GLE events.
3. If the injection time coincides with the start of a type II radio burst, it is possible that a CME-driven shock wave produces relativistic particles with energies $\geqslant$1 GeV.
4. If the flare procures enough relativistic energy but the injection time lies within the CME-driven shock wave, it is uncertain whether the energy released from the flare can cause the GLE. In this case, one can compute the possible relativistic energy for each energy band to check whether any fractional amount of energy might have been contributed to the shock acceleration.

Satisfying the criteria mentioned above, the key results are as follows.

a. For GLE69, the energy released from particle acceleration in a flare procured sufficient possible relativistic energy ($\sim$1.619 GeV).
b. For GLE70, the energy released from particle acceleration in a shock wave procured sufficient possible relativistic energy ($\sim$1.231 to $\sim$2.017 GeV) while any fractional amount of energy ($\sim$0.226 to $\sim$0.694 GeV) from preceding flare components might be considered as a contribution to the shock acceleration process.

Thus, we can conclude that GLE69 was most likely produced by the energy released from a solar flare while GLE70 was likely produced by the sum of the energy released mostly from a CME-driven shock and partially from preceding flare components.

We are grateful to the anonymous referee for constructive comments and valuable suggestions that helped us to develop this paper. We collected the data of GLEs from the NMDB which was founded under the European Union's FP7 program (contract No. 213007). To study the causes of GLEs, we analyzed the data/images of NGDC/NOAA, *ACE*, *Wind*-WAVES, *RHESSI*, *TRACE*, and *Hinode*. (*Hinode* is a Japanese mission launched by ISAS/JAXA collaborating with domestic partner NAOJ, and international partners NASA/STFC). This work was primarily initiated while thinking over a few comments made by Professor Brian R. Dennis on our previous work. Thanks to Dr. David J. Thompson for a comment on this work. One discussion with Professor K. Kudela on spectral index is recalled. Some discussions with Dr. Y. P. Li and Dr. Kim Tolbert on flare image processing were helpful. One discussion in 2010 with Dr. K. S. Cho on cosmic-ray transport effect is recalled. This work has been financed by the 973 program (2011CB811402) and NSFC grants (10833007, 11078025, and 11233008). Y.-J. Moon has been supported by the WCU Program (No. R31-10016) and by the Korea Research Foundation Grant (20090071744 & 20100014501) of the Korean Government (MOEHRD, Basic Research Promotion Fund). C. Li has been supported by the Natural Science Foundation (BK2012299) of Jiangsu province. We thank Dr. Z. Ning, Dr. S. Liu, and Dr. F. Melia for some discussions.

REFERENCES

Asai, A., Yokoyama, T., Shimojo, M., Masuda, S., & Shibata, K. 2006, J. Astrophys. Ast., 27, 167–173
Aschwanden, M. J. 2008, Asian J. Phys., 17, 423
Aschwanden, M. J. 2011, Space Sci. Rev.
Aschwanden, M. J., & Freeland, S. L. 2012, ApJ, 754, 112
Aschwanden, M. J., Kliem, B., Schwarz, U., et al. 1998, ApJ, 505, 941
Aschwanden, M. J., Schwartz, R. A., & Alt, D. M. 1995, ApJ, 447, 923
Bieber, J. W., Clem, J., Evenson, P., et al. 2008, in Proc. 30th ICRC (Mexico City), Vol. 1, 229
Bieber, J. W., Clem, J. M., Duldig, M. L., et al. 2004, J. Geophys. Res., 109, A12106
Bombardieri, D. J., Duldig, M. L., Humble, J. E., & Michael, K. J. 2008, ApJ, 682, 1315
Cane, H. V. 2002, in Proc. 27th ICRC (Hamburg), Vol. 8, 3231
Cane, H. V., Richardson, I. G., & von Rosenvinge, T. T. 2010, J. Geophys. Res., 115, A08101
Chupp, E. L., & Ryan, J. M. 2009, Res. Astron. Astrophys., 9, 11
Cliver, E. W. 2006, ApJ, 639, 1206
Cliver, E. W. 1996, in AIP Conf. Proc. 374, High Energy Solar Physics, ed. R. Ramaty, N. Mandzhavidze, & Z.-M. Hua (Melville, NY: AIP), 45
Cliver, E. W., Kahler, S. W., Shea, M.A., & Smart, D. F. 1982, ApJ, 260, 362
Firoz, K. A. 2006, in WDS, Part II, Physics of Plasmas and Ionized Media, ed. J. Safrankova & J. Pavlu (Prague: Charles University), 33
Firoz, K. A, Cho, K.-S., Hwang, J., et al. 2010, J. Geophys. Res, 115, A09105
Firoz, K. A., Hwang, J., Dorotovič, I., et al. 2011a, Astrophys. Space Sci., 331, 469
Firoz, K. A., Moon, Y.-J., Cho, K.-S., et al. 2011b, J. Geophys. Res., 116, A04101
Firoz, K. A, Moon, Y.-J., Park, S. H., et al. 2011c, ApJ, 743, 190
Gan, W. Q., Fang, C., & Zhang, H. Q. 1991, A&A, 241, 618
Gan, W. Q., Li, Y. P., & Miroshnichenko, L. I. 2008, Adv. Space Res., 41, 908
Gopalswamy, N., Hie, H., Yashiro, S., & Usoskin, I. 2005, in Proc. 29th ICRC (Pune), 3, 101
Grechnev, V. V., Kurt, V. G., Chertok, I. M., et al. 2008, Sol. Phys., 252, 149
Kahler, S. W. 1994, ApJ, 428, 837
Kahler, S. W. 2012, ApJ, 747, 66
Kallenrode, M.-B. 1993, J. Geophys. Res., 98, 19037
Kallenrode, M.-B., Cliver, E. W., & Wibberenz, G. 1992, ApJ, 391, 370
Klein, K.-L., Christian, S., Christian, T., et al. 2010, in Proc. 31st ICRC (Lodz), 1333
Klein, K.-L., Chupp, E. L., Trottet, G., et al. 1999, A&A, 348, 271
Klein, K.-L., Trottet, G., Samwel, S., & Malandraki, O. 2011, Sol. Phys., 269, 309
Kocharov, L., Saloniemi, O., Torsti, J., et al. 2007, ApJ, 659, 780
Kocharov, L., & Torsti, J. 2002, Sol. Phys., 207, 149
Kocharov, L. G., & Kovaltsov, G. A. 1986, in Proc. Int. School & Workshop on Plasma Astrophysics, ed. T. D. Guyenne (ESA-SP-251; Noordwijk: ESA), 101
Kudela, K., & Usoskin, I. 2004, Czech. J. Phys., 54, 239
Kumar, P., Srivastava, A. K., Somov, B. V., et al. 2010, ApJ, 723, 1651

Kuznetsov, S. N., Kurt, V. G., Yushkov, B. Y., et al. 2006, Contrib. Astron. Obs. Skalnate Pleso, 360, 85
Li, C., Dai, Y., Vial, J.-C., et al. 2009, A&A, 503, 1013
Li, C., Tang, Y. H., Dai, Y., et al. 2007, A&A, 472, 283
Li, Y. P., & Gan, W. Q. 2006, ApJ, 652, L61
Mann, G., Classen, T., & Aurass, H. 1995, Astron. Astrophys., 295, 775
Martirosyan, H., & Chilingarian, A. 2005, in Proc. 29th Int. Cosmic Ray Conf., Correlation of the Estimated Arrival Time of the Relativistic Solar Ions at 1 AU and Start of Ground Level Enhancement (GLE), ed. B. Sripathi Acharya, S. Gupta, P. Jagadeesan, A. Jain, S. Karthikeyan, S. Morris, & S. Tonwar (Mumbai: Tata Institute of Fundamental Research), 285
Masson, S, Klein, K.-L., Butikofer, R., et al. 2009, Solar Phys., 257, 305
Matthiä, D., Heber, B., Reitz, G., et al. 2009, J. Geophys. Res., 114, A08104
Mavromichalaki, H., Papaioannou, A., Plainaki, C., et al. 2011, Adv. Space Res., 47, 2210
McCracken, K. G., & Beer, J. 2008, in Proc. 30th ICRC (Mexico City), Vol. 1, 549
McCracken, K. G., Moraal, H., & Stoker, P. H. 2008, J. Geophys. Res., 113, A12101
Miroshnichenko, L. I. 2001, Solar Cosmic Rays (Dordrecht: Kluwer), 17 (ch.1)
Miroshnichenko, L. I., Vashenyuk, E. V., Balabin, Yu. V., et al. 2009, in Proc. 31st ICRC (Lodz), 1171
Moon, Y.-J., Chae, J., Choe, G. S., et al. 2004, J. Korean Astronomical Soc., 37, 41–53
Moon, Y.-J., Kim, Y.-H., Park, Y.-D., et al. 2007, PASJ, 59, 625
Moon, Y.-J., Yun, H. S., Lee, S. W., et al. 1999, in Sol. Phys., 184, 323
Moraal, H., McCracken, K. G., & Stoker, P. H. 2008, in Proc. 30th ICRC (Mexico City), Vol. 1, 265
Perez-Peraza, J., Gallegos, A., Vashenyuk, E. V., & Miroshnichenko, L. I. 1991, in Proc. 22nd ICRC (Dublin), 3, 5
Perez-Peraza, J., Gallegos-Cruz, A., Vashenyuk, E. V, et al. 2006, Adv. Space Res., 38, 418
Perez-Peraza, J., Vashenyuk, E. V., Gallegos-Cruz, A., et al. 2008, Adv. Space Res., 41, 947
Perez-Peraza, J., Vashenyuk, E. V., Miroshnichenko, L. I., et al. 2009, ApJ, 695, 865
Reames, D. V. 1999, Space Sci. Rev., 90, 413
Reames, D. V. 2009a, ApJ, 693, 812
Reames, D. V. 2009b, ApJ, 706, 844
Schlickeiser, R., & Miller, J. A. 1998, ApJ, 492, 352
Simnett, G. M. 2006, A&A, 445, 715
Simnett, G. M. 2007, A&A, 472, 309
Simnett, G. M., & Roelof, E. C. 2005, in Proc. 29th ICRC (Pune), 1, 233
Vashenyuk, E. V., Balabin, Y. V., Germanenko, A. V., & Gvozdevsky, B. B. 2011, Astrophys. Space Sci. Trans., 7, 453
Vashenyuk, E. V., Balabin, Y. V., & Gvozdevsky, B. B 2003, Proc. 28th ICRC (Lodz), 3401
Vashenyuk, E. V., Balabin, Y. V., & Gvozdevsky, B. B. 2009, in Proc. 31st Int. Cosmic Ray Conf., http://icrc2009.uni.lodz.pl/proc/pdf/icrc1304.pdf
Vashenyuk, E. V., Fischer, S., & Gvozdevsky, B. B. 1993, in 23rd Int. Cosmic Ray Conf., Vol. 3, Short Term SCR Intensity Variations During GLE, ed. D. A. Leahy, R. B. Hickws, & D. Venkatesan (Singapore: World Scientific), 266
Wang, H., Qiu, J., Jing, J., & Zhang, H. 2003, ApJ, 593, 564
Wang, R. G. 2009, Astropart. Phys., 31, 149
Wang, R. G., & Wang, J. X. 2006, Adv. Space Res., 38, 489
Warren, P. H., & Antiochos, S. K. 2004, ApJ, 611, L49